Article

Asymmetric, Nearly Barrierless C(sp3)-H Activation Promoted by Easily-Accessible N-protected Aminosulfoxides as New Chiral lig-ands

Soufyan Jerhaoui, Jean-Pierre DJUKIC, Joanna Wencel-Delord, and Françoise Colobert

ACS Catal., **Just Accepted Manuscript** • DOI: 10.1021/acscatal.8b04946 • Publication Date (Web): 04 Feb 2019

Asymmetric, Nearly Barrierless C(sp^3)-H Activation Promoted by Easily-Accessible *N*-protected Aminosulfoxides as New Chiral ligands

Soufyan Jerhaoui,[a] Jean-Pierre Djukic,[b] Joanna Wencel-Delord*[a] and Françoise Colobert*[a]

a) Laboratoire d'Innovation Moléculaire et Applications, ECPM, UMR 7042, Université de Strasbourg/Université de Haute – Alsace, 25 rue Becquerel, 67087, Strasbourg Cedex; b) Institut de Chimie de Strasbourg, UMR 7177, Université de Strasbourg

ABSTRACT: Although chiral sulfoxides are important motifs in medicinal chemistry and asymmetric synthesis, design and applications of sulfoxide ligands are still limited, in particular in the context of asymmetric C-H activation. We disclose herein the conception and synthesis of enantiopure N/S ligands: *N*-protected aminosulfoxides. The potential of these auxiliaries in asymmetric C(sp^3)-H activation is demonstrated as high enantioselectivity is reached during a Pd-catalyzed direct arylation of cyclopropane carboxylic acid derivatives. Besides, the capacity of these ligands goes far beyond as yet unknown direct alkynylation could also be performed with enantiomeric ratio up to 92:8. The preliminary mechanistic studies shed light on their original mode of action; key non-covalent interactions between the chiral complex and the substrate allows stabilization of agostic M-H-C interaction and π-stacking ligand-substrate bonding. DFT investigations suggest that, thanks to this unusual ligand/substrate activation, commonly recognized as difficult, the cleavage of the C-H bond is virtually barrier-less.

KEYWORDS: asymmetric C-H, enantioselective C(sp^3)-H activation, aminosulfoxide, DFT investigations, cyclopropane

1. INTRODUCTION

Chiral sulfoxides are important structures, present in natural products and biologically active compounds.[1] Moreover, stereogenic sulfinyls have established themselves as very powerful chiral auxiliaries for a large panel of diastereoselective transformations.[2] Chiral character of the sulfur atom combined with its strong coordinating properties and high configurational stability render this motif also an appealing candidate for the design of original chiral ligands (Scheme 1A). Accordingly, over the last two decades it has been shown that enantiopure bisulfoxide ligands are efficient chiral inductors for reactions such as Rh-catalyzed 1,4-conjugate additions[3] whereas phosphine/sulfoxide,[4] olefin/sulfoxide[5] and oxazoline/sulfoxide ligands[6] are able to coordinate Pd, thus enhancing asymmetric allylic alkylation. However, the design of conceptually new sulfoxide-based ligands has remained a rather niche topic, in particular regarding C-H activation.[7]

In 2007 White has demonstrated a unique activity of Pd-bis-sulfoxide complex for direct C-H activation of allylic substrates, thus showcasing that sulfoxides might be of great interest for the development of an extremely challenging field of asymmetric C-H activation (Scheme 1B-a).[8] Design of a stereoselective version of such a coupling turned out to be puzzling and an intramolecular direct allylic C-H activation/C-O coupling sequence was disclosed recently (Scheme 1B-b).[9] In this elegant isochromans' synthesis, oxazoline/sulfoxide ligand was crucial to reach high efficiency and stereoselectivity. Besides, the same family of chiral auxiliaries was applied for a rare example of atroposelective direct arylation (Scheme 1B-c).[10] In clear contrast, chiral sulfoxide ligands have never been used in direct enantioselective functionalization of unbiased C(sp^3)-H bonds.

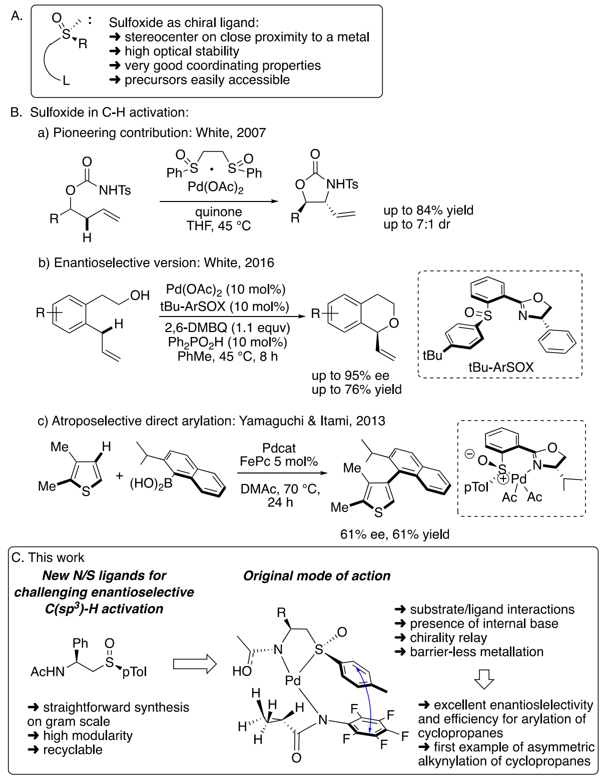

Scheme 1. Design of new sulfoxide ligands for asymmetric C(sp^3)-H activation.

Recently, our group has shown that a chiral sulfoxide moiety can be embedded in a bicoordinating N,S directing group, thus promoting stereoselective C(sp^3)-H activation of non-activated substrates.[11] Encouraged by these results and by the seldom applications of the sulfoxide ligands in the C-H activation reactions and following our program on asymmetric C-H activation using sulfoxide moiety,[12] we embarked on designing a conceptually new family of N/sulfoxides auxiliaries that might be able to induce an enantioselective metallation of non-activated C(sp^3)-H bonds (Scheme 1C). Our initial hypothesis surmised that the sulfoxide ligand might showcase a particular mode of action by establishing non-binding interactions with the substrate. Such a « substrate activation » via π-stacking should facilitate and direct the C-H activation step by guaranteeing spatial proximity. Besides, the presence of the N-coordinating moiety should promote the C-H abstraction step by acting as an internal base. Finally, a chirality relay between the C-stereogenic center and the N-coordinating motif could be expected thus giving a promise of an efficient stereoinduction.

2. RESULTS AND ANALYSIS

Our experimental efforts began by synthesizing a small library of original S/N ligands (Scheme 2). Initially, an aromatic ligand **L1**, showing a rigid architecture and featuring both, C-central chirality and enantiopure S-atom was synthesized using enantiopure benzylamine as a starting material.[13] Besides, surmising that a certain flexibility of the ligand might be required to accommodate both N and S liganding sites during coordination of Pd, a selection of more flexible, linear auxiliaries have been prepared. Firstly, a simple ethane linkage was installed between N and S atoms (**L2**) and progressively a second chirality element was introduced (**L3**). These original ligands have been prepared using a rapid and robust protocol employing enantiopure sulfinate precursor.[14] This efficient 4-steps synthesis involves initial imine formation between an aldehyde and *para*-methoxyaniline followed by nucleophilic addition of in situ deprotonated (*R*)-1-methyl-4-(methylsulfinyl)benzene occur smoothly, delivering the expected stereogenic amine in high diastereoselectivity (typically 9:1) and efficiency. Purification by recrystallization delivers a ligand direct precursor as a single diasteromer and final deprotection and protection sequence furnishes optically pure *N*-protected aminosulfoxides. Using this modular protocol, **L3-L13** were synthesized by varying: 1) substituents on the aliphatic backbone, 2) steric and electronic features of the sulfoxide moiety and 3) nature of N-protecting group. With thus synthesized library of new chiral ligands, we embarked on their evaluation in asymmetric C(sp^3)-H activation.[15],[16]

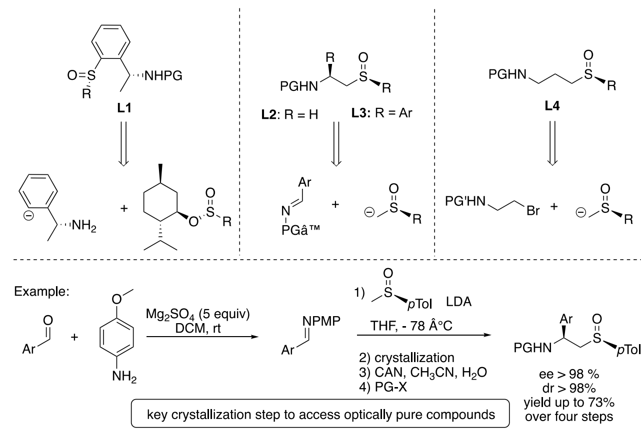

Scheme 2. Synthesis of N/Sulfoxide ligands.

Regarding prevalence of small cyclopropanes in natural products and biologically active scaffolds,[17] direct arylation of **1a** was selected as a test reaction (Scheme 3). It should be highlighted that although direct enantioselective arylation of cyclopropanes has already been disclosed, specially designed substrates such as cyclopropylmethylamines[18] or cyclopropanecarboxamides bearing a quaternary carbon[19] were required whereas functionalization of simple cyclopropanecarboxylates has been achieved only recently.[20]

Encouragingly, **L1**, in combination with Pd(TFA)$_2$ is able to promote this challenging direct coupling, albeit the desired product was isolated in low, 25% yield and enantioselectivity of 70:30 (Scheme 3). Comparable results were obtained when using the more flexible **L2**, but a remarkable improvement was witnessed when conducting the reaction with **L3**, bearing an additional stereocenter. In this case the arylated cyclopropane was delivered in 90% yield and 85:15 er. Interestingly, the expensive directing group (CONH(4-CF$_3$-2,3,5,6-C$_6$F$_4$), substrate **1a**) could be replaced by a more economic pentafluoroamide (substrate **1b**) without altering the efficiency of the catalytic system whereas simple benzylamide directing group (**1c**) failed. Interestingly, when **dia-L3** was used, the reaction occurred with the same stereoselectivity and efficiency, furnishing the opposite enantiomer of **3**; thus indicating the key role of the C-stereogenic center of the ligand. Further ligand screening showed that more flexible **L4**, generating upon coordination with Pd a 6-member chelate, performed poorly. Increased steric hindrance on the sulfoxide moiety (**L5**) and a rigidified aliphatic backbone (**L6**) were detrimental to both, reactivity and stereoselectivity. Subsequently, the impact of the N-protecting group was evaluated (**L7**-**L9**). TFA-protected ligand **L7** turned out to be slightly less efficient, but the desired product was isolated with a comparable optical purity. In contrast, in a presence of **L8** and **L9**, bearing respectively Boc and PMP protecting groups, only low conversions were measured. Finally, the steric and electronic properties of the phenyl group on **L3** were surveyed. Introduction of a sterically hindering substituent such as Me or CF_3 at *para*-position or 2-naphthyl-derived ligand allowed further increase of the stereoselectivity up to 90:10 (**L10-12**). Finally, optimal results were obtained using **L13** bearing sterically demanding *t*Bu moiety; the expected product was thus isolated with 94:6 e.r. and 75% conversion.

With the optimal ligand in hand, reaction conditions were optimized.[21] Use of a mixture of hexane and chloroform was beneficial for the chirality control but a change of silver salt from Ag_2CO_3 to AgOAc or AgTFA almost totally shut down the reactivity. Addition of NaTFA further promoted the reactivity while decreasing the excess of Ar-I coupling partner. Finally, arylation of **1b** delivered **3** in 78% isolated yield and e.r. of 96:4 when using 10 mol% of $Pd(TFA)_2$ in combination with 15 mol% of ligand, 2 equivalents of Ag_2CO_3 and 50 mol% of NaTFA, in hexane/chloroform mixture at 80 °C over 24h.

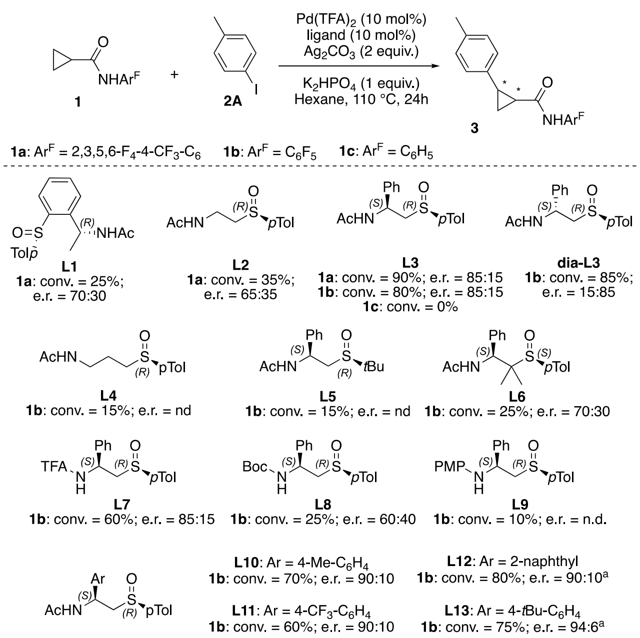

Scheme 3 Ligand optimization

This enantioselective direct $C(sp^3)$-H arylation turned out to be highly tolerant to a large panel of aryl iodides (Scheme 4). Arylation with simple iodobenzene (**4**) was as efficient as the coupling with both, electron-rich *p*-iodotoluene (**3**), and aromatics bearing electron withdrawing moieties such as CF_3, CO_2Me or Ac, delivering the functionalized products with up to 95% ee (**5**-**7**). In contrast, decreased stereoselectivity was observed for the CN-substituted Ar-I (**8** isolated with 85:15 e.r.). *Meta*-substituted Ar-I also performed remarkably well; Br-substituted **9** was isolated in 58% yield and e.r. of 95:5 and a comparable stereoinduction was reached for aryliodides bearing NO_2-moieties (**10** and **11**). Biologically relevant fluorinated motifs such as CF_3 (**13**) and OCF_3 (**14**) are well tolerated. The high reactivity of this catalytic system is further highlighted by a possible coupling with challenging *ortho*-substituted Ar-I, as witnessed by formation of **18** and **19** in excellent yields and high stereopurity.

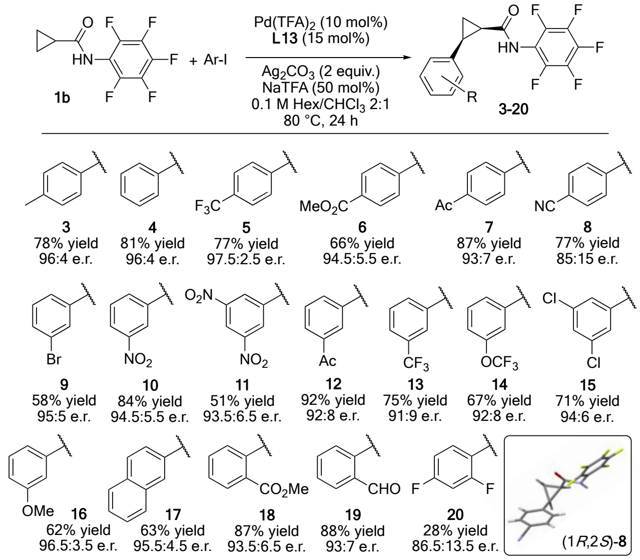

Scheme 4. Scope of arylation.

One of the important features of new ligands is their potential to promote few distinct transformations. Accordingly, the amino-sulfoxide **L13** was evaluated in asymmetric alkynylation that has not yet been reported for the cyclopropane substrate. Initially **1b** was reacted with (bromoethynyl)triisopropylsilane **21-Br**. Unexpectedly, under the reaction conditions previously optimized, an original cyclized compound **23** was isolated as a major product (Scheme 5a). Notably, when switching to the iodinated partner, ie. (iodoethynyl)triisopropylsilane **21-I**, the outcome of the reaction was altered and further fine tuning of the reaction protocol allowed synthesis of non-cyclized alkynylated cyclopropane **22** in more than 10:1 selectivity, 73% isolated yield and 92:8 e.r. (Scheme 5b). *Tert*-butyl(iodoethynyl)dimethylsilane **24-I** delivered product **25** in a comparable enantiopurity and high yield.

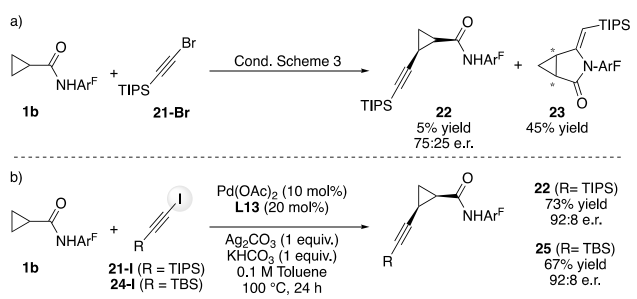

Scheme 5. Asymmetric direct alkynylation of cyclopropanes.

Subsequently, the removal of the amide auxiliary was studied (Scheme 6).[11] Under the previously developed conditions **10** was converted into the chiral cyclopropane ester **26** in 90% yield with no modification of the optical purity. Further recrystallization allowed almost total enantiomeric enrichment (Scheme 6a) thus this *cis*-substituted cycloproprane was buildup with ee > 99.5%. Structural X-ray diffraction analysis[22] of **26** confirmed the absence of epimerization of the stereocenters in the cyclopropane ring. Besides, a large-scale arylation of **1b** proceeded smoothly and the coupling product **16** underwent hydrolysis and following esterification under Yu's conditions[23] provided 552 mg (63% yield) of the ester **27** (Scheme 6b).

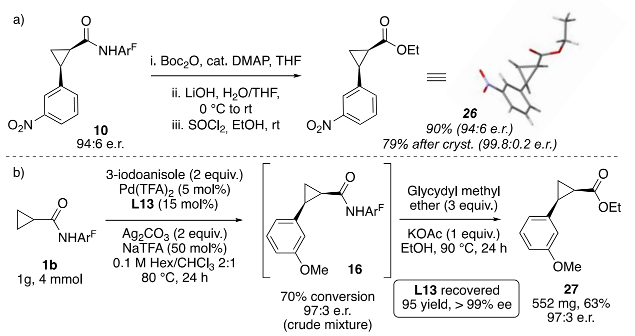

Scheme 6. Cleavage of the auxiliary and large-scale synthesis.

3. DISCUSSIONS

3.1. Preliminary mechanistic insights on the formation of the active catalyst species.

The efficient stereoinduction observed during the functionalization of cyclopropane rings suggests the initial formation of an active catalyst **cat-Pd-L13** from $Pd(TFA)_2$ and **L13** [24] In accordance with this hypothesis, formation of binuclear **cat-Pd-L13** was observed when mixing the palladium source and the ligand but addition of silver carbonate was crucial to achieve full conversion into the desired chelate (Scheme 7) as indicated by NMR, IR and HR-MS analysis. This structure quite clearly shows the expected bidentate S,N coordination and formation of a pseudo-planar five-membered ring. Absolute configuration of **L13** imposes both, Ar-substituent on C-stereocenter and *p*Tol-motif at S-stereocenter, to point in the same direction. Besides, the monomeric Pd/**L13** units are bridged with μ–trifluoroaceto group.

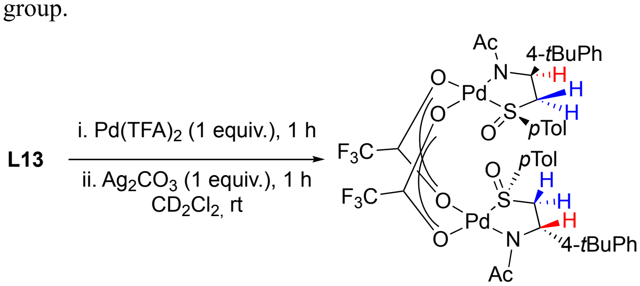

Scheme 7. Synthesis of dimeric Pd/L13 complex.

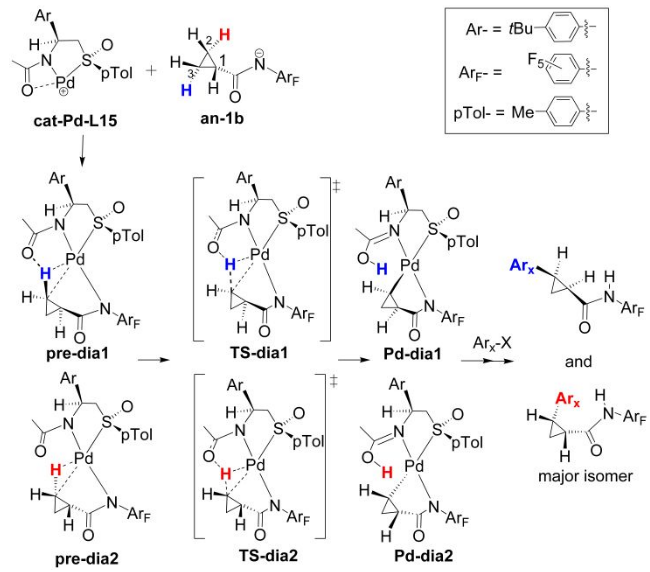

Scheme 8 Putative mechanism of the exogenous-base-less C-H bond activation promoted by the ancillary acetyl group at Pd-bound L13

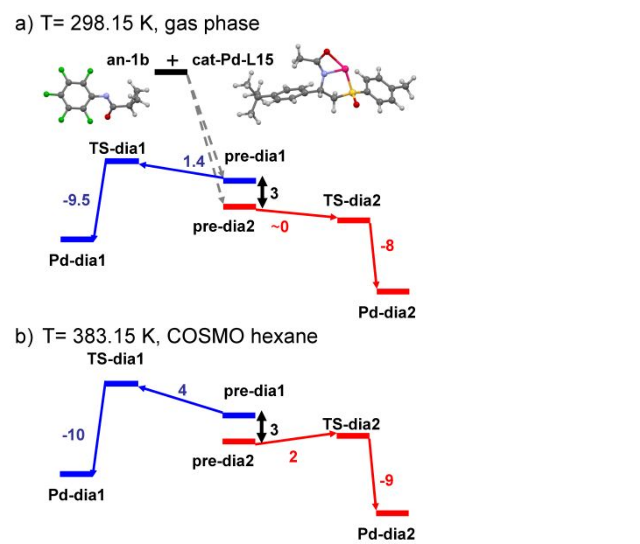

Figure 1. **Gibbs energy (in kcal/mol) profiles for the conversion of pre-dia1 and pre-dia2 into the heteroleptic bischelated Pd complexes Pd-dia1 and Pd-dia2 a) in the gas phase at T= 298.15 K and b) in COSMO[30] (hexane) at 383.15 K.**

3.2. DFT investigation of the C-H bond activation step.

Considering the unprecedented architecture of this ligand, DFT-based mechanistic studies were subsequently undertaken to elucidate the mechanism of this coupling. For the purpose of this study the recourse to DFT-D3[25]was considered mandatory as the stability of the key agostic reactive complexes, which are generally considered to take a central part into the C-H bond activation, strongly depends on the attractive contribution of London force (also known as dispersion).[26] All calculations were carried out at the ZORA[27]-PBE[28] -D3(BJ)[25]/all electron TZP level (cf. details in the SI), which has already shown good performance in modeling transition metal organometallic systems.[29] For comparison purposes thermodynamic parameters, that is mainly Gibbs energy variations ΔG were computed for models in the gas phase at 298.15 K (1 atm) and for models optimized by accounting solvation by the COSMO[30] model parametrized for *n*-hexane at 383.15 K (1 atm) (Figure 1).

The key C-H bond activation reaction was computed for the arylation of the amidate arising from **1b** in the presence of **L13**. It was surmised that enantioselectivity is controlled during the C-H activation step, when heteroleptic bischelated Pd intermediates **Pd-dia1** and **Pd-dia2** are formed.

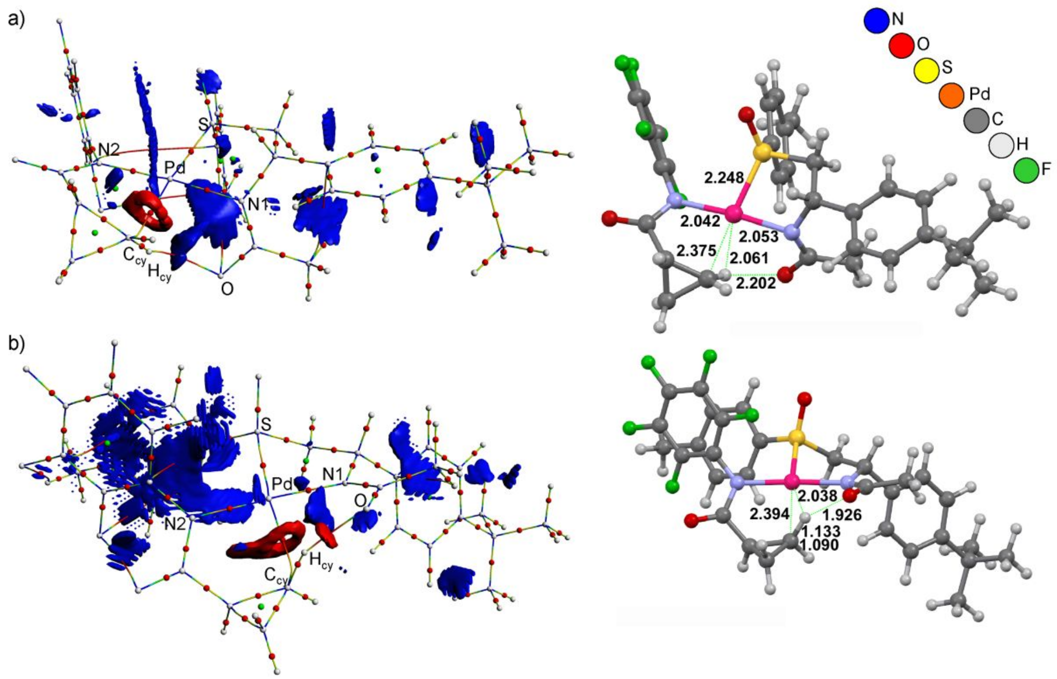

Figure 2 Gas phase models of pre-dia1-2 were optimized by DFT-D at the ZORA-PBE-D3(BJ)/all electron TZP level (see SI for NCI plots for COSMO-DFT models) and analyzed by QTAIM and NCI methods: a) joint QTAIM and NCI plots[31] of noncovalent interactions for pre-dia1, b) joint QTAIM and NCI[31] plots for pre-dia2. NCIs are materialized by reduced density gradient isosurfaces (cut-off value *s*= 0.02 a.u., ρ= 0.05 a.u.) colored according to the sign of the signed density $\lambda_2\rho$ (red colored fonts, in Å) : NCI isosurfaces are colored in red and blue for attractive and repulsive (or non bonded) NCI respectively. Significant interatomic distances (in Å) and atom color codes are detailed on the right hand side models. QTAIM analysis resulted on a series of bond paths (materialized by rainbowed lines), ring critical points (materialized by green dots) and bond critical points (3,-1) (materialized by red dots).

In principle this assumption requires, prior to the carbonyl-assisted C-H bond activation,[32] the formation of reactive complexes **pre-dia1** and **pre-dia2** wherein Pd-C-H "agostic"[33] interactions[34] result from palladium's interaction with C-H bonds of cyclopropyl's 2 and 3 positions (Scheme 8 and Figure 1) positioned cis with respect to the carbonyl group. Agostic interactions are indeed suspected to establish prior to effective C-H bond activation.[35] Assuming the model reaction of amidate **an-1b** with cationic Pd chelate **cat-Pd-L13** (Scheme 8), computation shows that the formation of **pre-dia2** is slightly more exoergonic than that of **pre-dia1** by only 3 kcal/mol whether computed in the gas phase at 298.15 K or when solvation was accounted for with the COSMO framework at 383.15K, that is the actual temperature of the catalysis taking place in a sealed vessel; the overall Gibbs enthalpy ΔG (298.15 K, 1 atm.) for this model step being ~ -100 kcal/mol (Figure 1).

QTAIM and NCI investigation of the reactive complexes.

The joint analysis of the bonding structure within gas-phase models of **pre-dia1-2** intermediates by the quantum theory of atoms in molecule (QTAIM[36]) and the intuitive non-covalent interaction (NCI[31]) plot method reveals the two-sided nature of the C-H-to-Pd interaction, i.e its covalent and non-covalent nature. Indeed, QTAIM analysis indicates that bond paths (BP) and critical points BCP (3,-1) exist between the cyclopropylic carbon atom C_{cy} and the Pd centre and between the C_{cy}-bound H atom and the proximal acetyl's oxygen atom. In contrast, no interactions have been demonstrated between the carbon-bound H_{cy} atom and the Pd centre. Table 1 lists the most significant informations extracted from the QTAIM study, i.e densities ρ and the negative laplacian of the density $-\frac{1}{4}\nabla^2\rho$ at bond critical points (3,-1), and from the analysis of related atomic Bader charges *q* and Mayer bond orders *m*. The electron density ρ at those critical points is slightly lower than for other coordination bonds that involve the Pd centre with amido and sulfoxide-type ligands. However the situation encountered here suggests that the acetyl moiety has a central role as an intramolecular proton scavenger actively involved in the C-H bond activation already in the early stage of the reactive complex.

An intuitive way of depicting this peculiar "agostic situation" would be that of an intramolecularly base-assisted palladation of the polarized $C_{cy}(\delta-)$-$H_{cy}(\delta+)$ bond matching the general so-called CMD mechanism, i.e the concerted carbon metallation-deprotonation. Scrutiny of so-called Bader atomic charges for the main atoms involved in the C_{cy}-H_{cy} bond activation, namely Pd, C_{cy}, H_{cy} and O (Table 1) support the hypothesis that the non-covalent component of the agostic interaction bears an ionic character. In fact for all cases of reactive complexes displayed in Table 1 the Pd-C_{cy} bond bears the properties of a typical ionic bond with $-1/4\nabla^2\rho<0$ and a low value of ρ in the 10^{-2} order.[37] Quite interestingly the NCI isosurfaces in both **pre-dia1** and **pre-dia2** display clearly an attractive component in the Pd-C_{cy} interspace (Figure 2), notwithstanding the type of models considered (either gas-phase or COSMO "solvated", cf. SI). This red-colored reduced density gradient isosurface perpendicular to the Pd-C_{cy} segment contains a hole typical of those situations[38] where a weak charge transfer interaction is supported by attractive NCIs. In this case the C_{cy}-Pd bond path passes through this "hole" and the associated BCP is positioned in its center. Furthermore, in **pre-dia2** an attractive NCI isosurface is present in the H_{cy}-O segment, exactly positioned at a BCP, whereas in **pre-dia1** the same NCI isosurface is non-bonding, illustrating the active role of the acetamido group.

Comparison of ρ values at BCPs and Mayer bond orders m[39] of **pre-dia1** and **pre-dia2** suggests that the C_{cy}-H_{cy} bond is significantly weaker in **pre-dia2** than in **pre-dia1**. This is consistent with the interatomic distance that is more elongated in **pre-dia2** (C_{cy}-H_{cy}= 1.133 Å, Pd-H_{cy}= 2.038 Å, Pd-C_{cy}= 2.394 Å, H_{cy}-O= 1.926 Å) than in **pre-dia1** (1.119 Å). Consistently the H_{cy}-O interaction is slightly stronger in **pre-dia2** (m in **pre-dia2** is two-fold that in **pre-dia1**). These slight differences outline the predisposition of **pre-dia2** to undergo palladation due to the fact that the vicinal acetyl group contributes to the polarization of this C-H bond and facilitates the transfer of H_{cy} onto the O centre. Extended transition state-natural orbital for chemical valence analysis[40] (abbr. ETS-NOCV, cf Supporting Information for details), a fragment-based orbital interaction analytical method, provides further confirmation of the charge transfer operating from the C_{cy}-H_{cy} bond to the Pd center (cf SI for details) and complements the results of QTAIM.

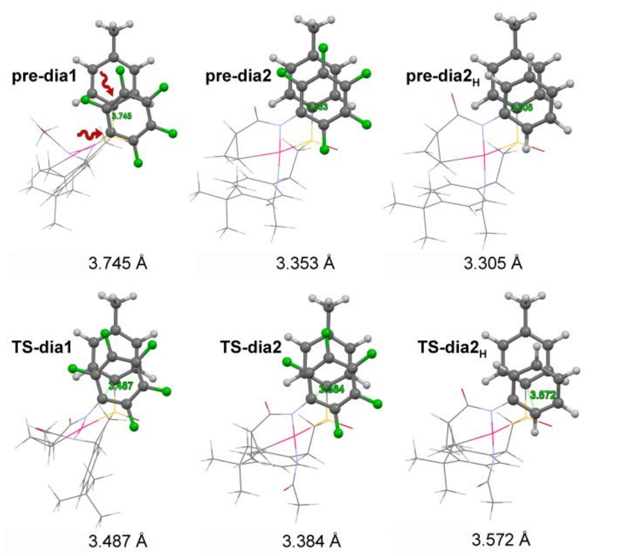

Figure 3 π–π interactions between the pentafluorophenyl and the tolyl groups in pre-dia1, pre-dia2, pre-dia2H, TS-dia1, TS-dia2, TS-dia2H: values of C_{ipso}-C_{ipso} distances are given below each representation. The red arrow designates the considered C_{ipso} positions.

Note that in all models some π-stacking of the C_6F_5 and p-tolyl groups (Figure 3) allegedly contributes to the stabilization of the already electronically favored *trans* N-Pd-N stereochemistry, which by the way is also the only one relevant in the CMD mechanism for it brings the cyclopropyl and acetyl group in close vicinity. It has been reported by Tsuzuki et al.[41] that the hexafluorobenzene-benzene slipped parallel complex is expected to have a calculated interaction energy twice as large as that of the dibenzene dimer due to dominant dispersion and electrostatic-based attractive interactions.[12] This feature of fluoroarene-arene[42] interactions might well be of importance in both reactive complexes studied here and might contribute to the cohesion of **pre-dia1** and **pre-dia2**. However, it must be stressed that the inter-arene stacking in **pre-dia1** is significantly less optimal than in **pre-dia2** as the C_6F_5 moiety only partly overlaps with the tolyl group: the C_{ipso}-C_{ipso} distance separating the tolyl ring from the pentafluorophenyl in **pre-dia1** (3.745 Å) is significantly longer than that in **pre-dia2** (3.363 Å), wherein the slightly staggered inter-arene parallel overlap is more optimal. For the purpose of comparison the analogue of **pre-dia2** wherein all F atoms were replaced by H atoms, i.e. **pre-dia2$_H$**, was computed and submitted to QTAIM and NCI analyses (Table 1). As shown in Table 1 the replacement of F atoms by H results in slight changes in the electron density topology in the Pd-C_{cy}-H_{cy} motif. Although in **pre-dia2$_H$** the Pd-C_{cy} interaction remains roughly identical from the view point of ρ and m parameters to that in **pre-dia2**, the most significant change occurs in the H_{cy}-O interaction that bears a Mayer bond order m about half of that encountered in **pre-dia2** and a density at BCP by one third lower than in the fluorinated analog (Table 1).

It is speculated that this difference is the result of combined conformational strains and slightly lower polarization of the C_{cy}-H_{cy} bond in **pre-dia2$_H$**. It is not clear yet whether the presence of the remote C_6F_5 group is solely responsible for the peculiar property of the agostic C_{cy}-H_{cy} to Pd interaction though. The exoergonic conversion of **pre-dia1** and **pre-dia2** into **Pd-dia1** and **Pd-dia2** respectively involves transition states **TS-dia1** (gas phase model ν_{TS}= 403 $i$cm^{-1}, COSMO model ν_{TS}= 450 $i$cm^{-1}) and **TS-dia2** (gas phase model ν_{TS}= 415 $i$cm^{-1}, COSMO model ν_{TS}= 479 $i$cm^{-1}), in a quasi barrier-less fashion for **pre-dia2** (~0 kcal/mol in the gas phase at 298.15 K and 2 kcal/mol in the COSMO model at 383.15 K) and with a slightly higher Gibbs activation energy for **pre-dia1** though (1 kcal/mol in the gas phase at 298.15 K and 4 kcal/mol in the COSMO model at 383.15 K). In stark contrast with the accepted base-assisted Pd(II) C-H bond activation mechanism[32c] but in rather good accord with the mechanism proposed by Yu et al.[32b] for a different Pd(II) initiated alkyl C-H bond activation displaying a higher activation barrier of ca. 10 kcal/mol, it is now conspicuous that the migration of the "activated" H atom of the cyclopropyl to the vicinal acetylamido O atom occurs with the assistance of an attractive noncovalent H_{Cy}-Pd interaction in both **TS-dia1** and **TS-dia2** according to NCI isosurface plots (Figure 4a,b). The red isosurface located within the Pd-C_{cy}-O triangle is not related to any bond path or bond critical point. The QTAIM analysis of both **TS-dia1** and **TS-dia2** locates indeed quite expectedly BPs and BCPs for the Pd-C_{cy}, Pd-H_{cy} and O-H_{cy} interactions (cf SI for details).

Table 1. Selected parameters (negative of the laplacian of the density $-1/4\nabla^2\rho$, density at bond critical point ρ□@BCP(3,-1), Mayer bond order *m*, Bader atomic charges *q*) for the QTAIM analysis of reactive complexes and associated transition states pre(TS)-dia1-2

structure	bond path	$-1/4\nabla^2\rho$ @BCP(3,-1) (au)	ρ□@BCP(3,-1) (au)	*m*	$q(C_{cy})$, $q(H_{cy})$, $q(Pd)$, $q(O)$	structure	bond path	$-1/4\nabla^2\rho$ @BCP(3,-1) (au)	ρ@BCP(3,-1) (au)	*m*	$q(C_{cy})$, $q(H_{cy})$, $q(Pd)$, $q(O)$
pre-dia1					-0.15, 0.11, 0.60, -1.07	**TS-dia1**					-0.30, 0.33, 0.57, -1.03
	$Pd-C_{cy}$	-0.042	0.054	0.17			$Pd-C_{cy}$	-0.045	0.082	0.26	
	$C_{cy}-H_{cy}$	0.195	0.251	0.94			$C_{cy}-H_{cy}$	0.091	0.174	0.65	
	$H_{cy}-O$	-0.014	0.018	0.06			$H_{cy}-O$	-0.020	0.090	0.37	
pre-dia2					-0.16, 0.14, 0.60, -1.06	**TS-dia2**					-0.30, 0.33, 0.57, -1.03
	$Pd-C_{cy}$	-0.042	0.054	0.20			$Pd-C_{cy}$	-0.045	0.081	0.27	
	$C_{cy}-H_{cy}$	0.183	0.243	0.88			$C_{cy}-H_{cy}$	0.090	0.175	0.65	
	$H_{cy}-O$	-0.023	0.032	0.12			$H_{cy}-O$	-0.022	0.089	0.36	
pre-dia2$_H$					-0.12, 0.10, 0.60, -1.06	**TS-dia2$_H$**					-0.33, 0.34, 0.57, -1.03
	$Pd-C_{cy}$	-0.042	0.052	0.17			$Pd-C_{cy}$	-0.046	0.084	0.28	
	$C_{cy}-H_{cy}$	0.191	0.249	0.94			$C_{cy}-H_{cy}$	0.076	0.162	0.63	
	$H_{cy}-O$	-0.016	0.020	0.06			$H_{cy}-O$	-0.017	0.097	0.39	

3.3. Stereochemical model.

Elucidation of key factors governing the stereodiscrimination during an enantioselective transformation is generally highly challenging, when comparing rather small energy barriers that may lead to a favored formation of one enantiomer compared to the other. However, the experimental results combined with DFT calculations provide indications allowing to propose of a plausible stereochemical model for this asymmetric C(sp^3)-H activation. Firstly, electronic in nature factors governing the stereoselectivity have been uncovered via DFT calculations (Figures 1, 3) and summarized on Scheme 9a. The energy difference of **pre-dia1** and **pre-dia2** of ca. 3 kcal/mol was found, in agreement with experimentally observed enantioselectivity. Combination of several effects explains the preference given to **Pd-dia2** in the catalysis.

Based on the DFT calculations, the first effect is the optimal compactness and cohesion of reactive complex **pre-dia2**, which bears the tightest $\pi-\pi$ arrangement and the optimal *trans*-N-Pd-N coordination stereochemistry that brings the cyclopropyl moiety close to the acetamido moiety that acts as the internal base. It can be seen in Figure 3 that the $\pi-\pi$ stacking arrangement and C_{ipso}-C_{ipso} distances in the reactive complexes and transition states vary the most for **pre-dia1**, whereas π-stacking in **pre-dia2** remains mostly unchanged. Even though **TS-dia1** benefits from a better $\pi-\pi$ overlap than in its precursor reactive complex **pre-dia1**, the activation barrier remains slightly higher than for **pre-dia2**/**TS-dia2**.

The second effect is an optimal "agostic" C-H-Pd interaction benefiting from a polarization of the C_{cy}-H_{cy} bond by an effective interaction with the acetylamido side group that is stronger in **pre-dia2** than in **pre-dia1**. According to QTAIM data, in both reactive complexes the C_{cy}-H_{cy} bond is mostly a "covalent" bond, of "shared" character according to QTAIM; it is clearly weaker in **pre-dia2** than in **pre-dia1**. Its activation operates by an ionic interaction with the vicinal O center leading to a situation in the associated "early transition state" where still a significant "shared"(covalent) character remains. According to figure 4 that depicts NCI plots for both **TS-dia1** and **TS-dia2,** the migration of H atom from the aromatic carbon atom to the acetate's oxygen is attractively assisted by noncovalent interaction with the Pd center, which to the best of our knowledge is unprecedented. At this turning point, the driving exergonic formation of **Pd-dia1-2** is crucial to ensure thermodynamic irreversibility.

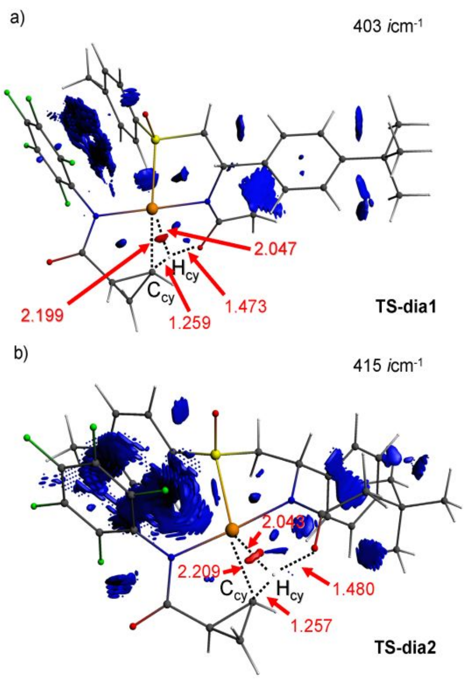

Figure 4. NCI isosurfaces[31a] in gas-phase models of TS-dia1 (a) and TS-dia2 (b) with significant interatomic distances and imaginary frequencies associated to the C_{cy}-H_{cy} bond activation assisted by the vicinal Pd and O centers. NCIs are materialized by reduced density gradient isosurfaces (cut-off value s= 0.02 a.u., ρ= 0.05 a.u.) colored according to the sign of the signed density $\lambda_2\rho$ (Significant interatomic distances are detailed in red colored fonts, in Å). Atom color code: Pd, orange, O, red, F green, S, yellow N blue, C grey. The red isosurface in the Pd-H_{cy} segment materializes the attractive non-covalent assistance of the Pd centre to the H_{cy} migration in the C-H bond activation process.

Finally, a supplementary important factor that may also be relevant is the topology or shape of **Pd-dia1** and **Pd-dia2**. Although being almost isoenergetic, **Pd-dia2** displays a marked helical distortion that tilts the 4-*tert*-butylphenyl group about 40-45° out of the mean coordination plane of the Pd center, whereas in **Pd-dia1**, the same aryl group remains roughly in the mean coordination plane. It is not yet clear how this marked distortion of the amidosulfoxide [N,S] ligand could create sufficient discrimination between these two palladacycles to consolidate the enantio-differentiation in the overall catalysis, which seemingly already favors **pre-dia2**. This difference of topology of **Pd-dia1** and **Pd-dia2** might result in slight differences of kinetic reactivity in the subsequent arylation step entailing stereochemical discrimination in the halogenoaryl oxidative addition to the Pd(II) center and in the last step, i.e. the reductive elimination step. This point will be addressed elsewhere. Nonetheless, it must be also stressed that a comparison of gas phase models of **pre-dia2** and **pre-dia2$_H$** considering the interaction of the cation **cat-Pd-L13** and anions **an-1b** and **an-1b$_H$** in their so-called prepared geometry indicates that in reactive complex **pre-dia2$_H$** the F-devoid **an-1b$_H$** ligand is more tightly bound to the Pd center than **an-1b** by 8 kcal/mol, a significant difference that points the role of the pentafluorophenyl group in **an-1b** : it induces a weaker amido-*N* bonding to Pd, which is crucial in ensuring catalytic turnover by allowing the ready decoordination of the functionalized substrate upon completion of the full catalytic cycle.

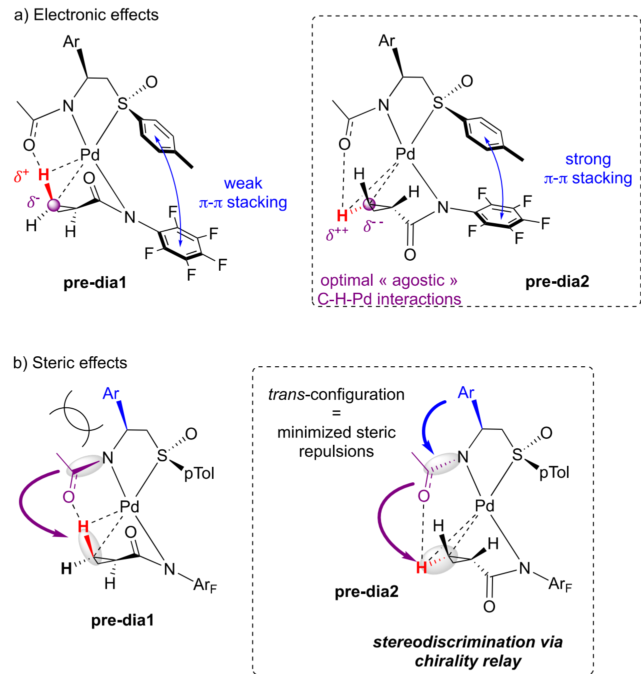

Scheme 9. Speculative stereomodel.

In addition to these mechanistic considerations, the experimental data provide complementary information about steric factors governing the stereoinduction. During the screening of different ligands it was observed that while **L13** induces excellent enantioselectivity of 94:6, its thioether analogue furnished the expected product as 75:25 enantiomeric mixture (cf Supporting Information for details). This result shows clearly that the chiral induction is mainly controlled by the C-stereogenic center of the ligand. Accordingly, a chirality relay from the ligand to the substrate might be expected (Scheme 9b).[43, 24c] For conformational reasons, the steric repulsion between the Ar substituent of the ligand, pointing upwards, and the N-Ac moiety, pushes acetyl below the Pd-coordination plane. As the acetyl moiety plays the role of an internal base and a proton shuttle actively involved in the metallation step, the proton downward would be abstracted to give the corresponding metallacycle intermediate. Worthy to note is that the optimal enantioselectivity achieved in the presence of **L13** could arise from the optimal steric repulsion between 4-*t*BuC_6H_4 motif and the N-Ac group, enhanced in presence of encumbering *t*Bu substituent. Moreover, such chirality relay is favored for **pre-dia2** due to the tightest π-stacking (Scheme 9a).

4. CONCLUSIONS

In conclusion, we report herein a new family of ligands for asymmetric C(sp^3)-H activation. Remarkably, these new auxiliaries are highly efficient and stereoselective allowing not only direct arylation, but also yet unprecedented alkynylation. DFT calculations further highlight a unique activity of this auxiliary, prompt to enhance a nearly barrier-less metallation event. Based on the in-depth mechanistic studies and the experimental results, the stereomodel for this transformation could be proposed to rationalize the excellent reactivity of this new family of ligands in extremely challenging stereodifferentiation of prochiral H-atoms. The basic comprehension of this catalytic system and factors governing stereoinduction, should allow us to achieve a more rational conception of challenging and alternative asymmetric C(sp^3)-H activation reactions.

ASSOCIATED CONTENT

SUPPORTING INFORMATION

The Supporting Information is available free of charge on the ACS Publications website.

Experimental data concerning synthesis of ligands, substrates and products. Analytical data concerning characterization of ligands, substrates and products (NMR, HRMS, chiral HPLC). Detailed optimization study. Supplementary Matarial concering DFT calculations.

AUTHOR INFORMATION

Corresponding Author

* E-mail: wenceldelord@unistra.fr; francoise.colobert@unistra.fr

Author Contributions

The manuscript was written through contributions of all authors. / All authors have given approval to the final version of the manuscript.

Funding Sources

Project ANR "Sulf-As-CH"

ACKNOWLEDGMENT

We thank the CNRS (Centre National de la Recherche Scientifique), the "Ministère de l'Enseignement Supérieur et de la Recherche", and ANR (Agence Nationale de la Recherche) France for financial support. Dr S. J. is very grateful to the ANR (Agence Nationale de la Recherche), France for a doctoral grant. We are also very grateful to Dr Lydia Karmazin and Corinne Bailly for single crystal X-ray diffraction analysis. We acknowledge Dr Quentin Dherbassy for fruitful discussions.

REFERENCES

(1) For selected general reviews on sulfoxides see: a) Fernández, I.; Khiar, N. Recent Developments in the Synthesis and Utilization of Chiral Sulfoxides. *Chem. Rev.* **2003**, *103*, 3651–3706. b) Pellissier, H. Use of Chiral Sulfoxides in Asymmetric Synthesis. *Tetrahedron* **2006**, *62*, 5559–5601.

(2) a) Otocka, S.; Kwiatkowska, M.; Madalińska, L.; Kiełbasiński, P. Chiral Organosulfur Ligands/Catalysts with a Stereogenic Sulfur Atom: Applications in Asymmetric Synthesis. *Chem. Rev.* **2017**, *117*, 4147–4181. b) Trost, B. M.; Rao, M. Development of Chiral Sulfoxide Ligands for Asymmetric Catalysis. *Angew. Chem., Int. Ed.* **2015**, *54*, 5026–5043. c) Sipos, G.; Drinkel, E. E.; Dorta, R. The Emergence of Sulfoxides as Efficient Ligands in Transition Metal Catalysis. *Chem. Soc. Rev.* **2015**, *44*, 3834–3860.

(3) For selected examples see: a) Chen, J.; Chen, J.; Lang, F.; Zhang, X.; Cun, L.; Zhu, J.; Deng, J.; Liao, J. A *C* $_2$ -Symmetric Chiral Bis-Sulfoxide Ligand in a Rhodium-Catalyzed Reaction: Asymmetric 1,4-Addition of Sodium Tetraarylborates to Chromenones. *J. Am. Chem. Soc.* **2010**, *132*, 4552–4553. b) Mariz, R.; Luan, X.; Gatti, M.; Linden, A.; Dorta, R. A Chiral Bis-Sulfoxide Ligand in Late-Transition Metal Catalysis; Rhodium-Catalyzed Asymmetric Addition of Arylboronic Acids to Electron-Deficient Olefins. *J. Am. Chem. Soc.* **2008**, *130*, 2172–2173. c) Chen, Q.-A.; Dong, X.; Chen, M.-W.; Wang, D.-S.; Zhou, Y.-G.; Li, Y.-X. Highly Effective and Diastereoselective Synthesis of Axially Chiral Bis-Sulfoxide Ligands via Oxidative Aryl Coupling. *Org. Lett.* **2010**, *12*, 1928–1931. d) Lang, F.; Chen, G.; Li, L.; Xing, J.; Han, F.; Cun, L.; Liao, J. Rhodium-Catalyzed Highly Enantioselective Addition of Arylboronic Acids to 2-Nitrostyrenes by Tert-Butanesulfinylphosphine Ligand. *Chem. Eur. J.* **2011**, *17*, 5242–5245. e) Lang, F.; Li, D.; Chen, J.; Chen, J.; Li, L.; Cun, L.; Zhu, J.; Deng, J.; Liao, J. Tert-Butanesulfinylphosphines: Simple Chiral Ligands in Rhodium-Catalyzed Asymmetric Addition of Arylboronic Acids to Electron-Deficient Olefins. *Adv. Synth. Catal.* **2010**, *352*, 843–846. f) Bürgi, J. J.; Mariz, R.; Gatti, M.; Drinkel, E.; Luan, X.; Blumentritt, S.; Linden, A.; Dorta, R. Unprecedented Selectivity via Electronic Substrate Recognition in the 1,4-Addition to Cyclic Olefins Using a Chiral Disulfoxide Rhodium Catalyst. *Angew. Chem., Int. Ed.* **2009**, *48*, 2768–2771.

(4) For selected examples see: a) Hiroi, K.; Suzuki, Y. New Chiral O-(Phosphinoamido)Phenyl Sulfoxide Ligands in Palladium-Catalyzed Asymmetric Allylic Alkylations. *Tetrahedron Lett.* **1998**, *39*, 6499–6502. b) Nakamura, S.; Fukuzumi, T.; Toru, T. Novel Chiral Sulfur-Containing Ferrocenyl Ligands for Palladium-Catalyzed Asymmetric Allylic Substitution. *Chirality* **2004**, *16*, 10–12. c) Chen, J.; Lang, F.; Li, D.; Cun, L.; Zhu, J.; Deng, J.; Liao, J. Palladium-Catalyzed Asymmetric Allylic Nucleophilic Substitution Reactions Using Chiral Tert-Butanesulfinylphosphine Ligands. *Tetrahedron: Asymmetry* **2009**, *20*, 1953–1956.

(5) For a review see: Li, Y.; Xu, M.-H. Simple Sulfur–Olefins as New Promising Chiral Ligands for Asymmetric Catalysis. *Chem. Commun.* **2014**, *50*, 3771–3782.

(6) For a selected review see: Allen, J. V.; Bower, J. F.; Williams, J. M. J. Enantioselective Palladium Catalysed Allylic Substitution. Electronic and Steric Effects of the Ligand. *Tetrahedron: Asymmetry* **1994**, *5*, 1895–1898.

(7) Pulis, A. P.; Procter, D. J. C−H Coupling Reactions Directed by Sulfoxides: Teaching an Old Functional Group New Tricks. *Angew. Chem. Int. Ed.* **2016**, *55*, 9842–9860.

(8) Fraunhoffer, K. J.; White, M. C. *Syn* -1,2-Amino Alcohols via Diastereoselective Allylic C−H Amination. *J. Am. Chem. Soc.* **2007**, *129*, 7274–7276.

(9) Ammann, S. E.; Liu, W.; White, M. C. Enantioselective Allylic C−H Oxidation of Terminal Olefins to Isochromans by Palladium(II)/Chiral Sulfoxide Catalysis. *Angew. Chem., Int. Ed.* **2016**, *55*, 9571–9575.

(10) Yamaguchi, K.; Kondo, H.; Yamaguchi, J.; Itami, K. Aromatic C–H Coupling with Hindered Arylboronic Acids by Pd/Fe Dual Catalysts. *Chem. Sci.* **2013**, *4*, 3753–3757.

(11) a) Jerhaoui, S.; Chahdoura, F.; Rose, C.; Djukic, J.-P.; Wencel-Delord, J.; Colobert, F. Enantiopure Sulfinyl Aniline as a Removable and Recyclable Chiral Auxiliary for Asymmetric C(sp^3)−H Bond Activation. *Chem. Eur. J.* **2016**, *22*, 17397–17406. b) Jerhaoui, S.; Djukic, J.-P.; Wencel-Delord, J.; Colobert, F. Stereoselective Sulfinyl Aniline-Promoted Pd-Catalyzed C−H Arylation and Acetoxylation of Aliphatic Amides. *Chem. Eur. J.* **2017**, *23*, 15594–15600. c) Jerhaoui, S.; Poutrel, P.; Djukic, J.-P.; Wencel-Delord, J.; Colobert, F. Stereospecific C–H Activation as a Key Step for the Asymmetric Synthesis of Various Biologically Active Cyclopropanes. *Org. Chem. Front.* **2018**, *5*, 409–414.

(12) a) Hazra, C. K.; Dherbassy, Q.; Wencel-Delord, J.; Colobert, F. Synthesis of Axially Chiral Biaryls through Sulfoxide-Directed

Asymmetric Mild C-H Activation and Dynamic Kinetic Resolution. *Angew. Chem., Int. Ed.* **2014**, *53*, 13871–13875. b) Dherbassy, Q.; Schwertz, G.; Chessé, M.; Hazra, C. K.; Wencel-Delord, J.; Colobert, F. 1,1,1,3,3,3-Hexafluoroisopropanol as a Remarkable Medium for Atroposelective Sulfoxide-Directed Fujiwara-Moritani Reaction with Acrylates and Styrenes. *Chem. Eur. J.* **2016**, *22*, 1735–1743. c) Dherbassy, Q.; Wencel-Delord, J.; Colobert, F. Asymmetric C–H Activation as a Modern Strategy towards Expedient Synthesis of Steganone. *Tetrahedron* **2016**, *72*, 5238–5245. d) Dherbassy, Q.; Djukic, J.-P.; Wencel-Delord, J.; Colobert, F. Two Stereoinduction Events in One C−H Activation Step: A Route towards Terphenyl Ligands with Two Atropisomeric Axes. *Angew. Chem., Int. Ed.* **2018**, *57*, 4668–4672.

(13) For details see SI.

(14) Zucca, C.; Bravo, P.; Corradi, E.; Meille, S.; Volonterio, A.; Zanda, M. On the Addition of Lithium Methyl p-Tolyl Sulfoxide to N-(PMP)-Aryladimines. *Molecules* **2001**, *6*, 424–432.

(15) For selected reviews on asymmetric C-H activation see : : a) Saint-Denis, T. G.; Zhu, R.-Y.; Chen, G.; Wu, Q.-F.; Yu, J.-Q. Enantioselective C(Sp ^{3}) – H Bond Activation by Chiral Transition Metal Catalysts. *Science* **2018**, *359*, 759-770. b) Zheng, C.; You, S.-L. Recent Development of Direct Asymmetric Functionalization of Inert C–H Bonds. *RSC Adv.* **2014**, *4*, 6173–6214. c) Ye, B.; Cramer, N. Chiral Cyclopentadienyls: Enabling Ligands for Asymmetric Rh(III)-Catalyzed C–H Functionalizations. *Acc. Chem. Res.* **2015**, *48*, 1308–1318. d) Newton, C. G.; Wang, S.-G.; Oliveira, C. C.; Cramer, N. Catalytic Enantioselective Transformations Involving C–H Bond Cleavage by Transition-Metal Complexes. *Chem. Rev.* **2017**, *117*, 8908–8976. e) Wencel-Delord, J.; Colobert, F. Asymmetric C(sp^2)-H Activation. *Chem. Eur. J.* **2013**, *19*, 14010–14017.

(16) For selected reviews on C(sp^3)-H activation see : a) Banerjee, Asarkar, S.; Patel, B. K. C–H Functionalisation of Cycloalkanes. *Org. Biomol. Chem*. **2017**, *15*, 505–530. b) He, J.; Wasa, M.; Chan, K. S. L.; Shao, Q.; Yu, J.-Q. Palladium-Catalyzed Transformations of Alkyl C–H Bonds. *Chem. Rev.* **2017, ***117*, 8754-8786. c) Qiu, G.; Wu, J. Transition Metal-Catalyzed Direct Remote C–H Functionalization of Alkyl Groups via C(Sp3)–H Bond Activation. *Org. Chem. Front.* **2015**, *2*, 169–178. d) Yang, X.; Shan, G.; Wang, L.; Rao, Y. Recent Advances in Transition Metal (Pd, Ni)-Catalyzed C(Sp3)H Bond Activation with Bidentate Directing Groups. *Tetrahedron Lett.* **2016**, *57*, 819–836. e) Baudoin, O. Ring Construction by Palladium(0)-Catalyzed C(Sp3)–H Activation. *Acc. Chem. Res*. **2017***, 50,* 1114–1123.

(17) For the selected reviews see: a) Mizuno, A.; Matsui, K.; Shuto, S. From Peptides to Peptidomimetics: A Strategy Based on the Structural Features of Cyclopropane. *Chem. Eur. J.* **2017**, *23*, 14394–14409. b) Talele, T. T. The "Cyclopropyl Fragment" Is a Versatile Player That Frequently Appears in Preclinical/Clinical Drug Molecules. *J. Med. Chem.* **2016**, *59*, 8712–8756. c) Donaldson, W. Synthesis of Cyclopropane Containing Natural Products. *Tetrahedron* **2001**, *57*, 8589–8627. d) Chen, D.-Y.; Pouwer, R. H.; Richard, J. -A. Recent advances in the total synthesis of cyclopropane-containing natural products. *Chem. Soc. Rev.* **2012**, *41*, 4631-4642. e) Fan, Y.-Y.; Gao, X.-H.; Yue, J.-M. Attractive natural products with strained cyclopropane and/or cyclobutene ring systems. *Sci. China Chem*. **2016**, *59*, 1126-1141.

(18) Chan, K. S. L.; Fu, H.-Y.; Yu, J.-Q. Palladium(II)-Catalyzed Highly Enantioselective C–H Arylation of Cyclopropylmethylamines. *J. Am. Chem. Soc.* **2015**, *137*, 2042–2046.

(19) Wasa, M.; Engle, K. M.; Lin, D. W.; Yoo, E. J.; Yu, J.-Q. Pd(II)-Catalyzed Enantioselective C–H Activation of Cyclopropanes. *J. Am. Chem. Soc.* **2011**, *133*, 19598–19601.

(20) Shen, P.-X.; Hu, L.; Shao, Q.; Hong, K.; Yu, J.-Q. Pd(II)-Catalyzed Enantioselective C(Sp ^{3})–H Arylation of Free Carboxylic Acids. *J. Am. Chem. Soc.* **2018**, *140*, 6545–6549.

(21) For further optimisation study see the SI.

(22) (1*R,2S*)**-8**: CCDC-1859147; contain the supplementary crystallographic data for this paper. These data can be obtained from the Cambridge Crystallographic Data.

(23) Pei, Q.-L.; Che, G.-D.; Zhu, R.-Y.; He, J.; Yu, J.-Q. An Epoxide-Mediated Deprotection Method for Acidic Amide Auxiliary. *Org. Lett.* **2017**, *19*, 5860–5863.

(24) a) Wu, Q.-F.; Shen, P.-X.; He, J.; Wang, X.-B.; Zhang, F.; Shao, Q.; Zhu, R.-Y.; Mapelli, C.; Qiao, J. X.; Poss, M. A.; et al. Formation of α-Chiral Centers by Asymmetric β-C(Sp ^{3})–H Arylation, Alkenylation, and Alkynylation. *Science* **2017**, *355* (6324), 499–503. b) Giri, R.; Lan, Y.; Liu, P.; Houk, K. N.; Yu, J.-Q. Understanding Reactivity and Stereoselectivity in Palladium-Catalyzed Diastereoselective Sp ^{3} C–H Bond Activation: Intermediate Characterization and Computational Studies. *J. Am. Chem. Soc.* **2012**, *134*, 14118–14126. c) Cheng, G.-J.; Chen, P.; Sun, T.-Y.; Zhang, X.; Yu, J.-Q.; Wu, Y.-D. A Combined IM-MS/DFT Study on [Pd(MPAA)]-Catalyzed Enantioselective C-H Activation: Relay of Chirality through a Rigid Framework. *Chem. Eur. J.* **2015**, *21*, 11180–11188.

(25) Grimme, S.; Ehrlich, S.; Goerigk, L. Effect of the damping function in dispersion corrected density functional theory. *J. Comp. Chem.* **2011**, *32*, 1456-1465. b) Grimme, S.; Antony, J.; Ehrlich, S.; Krieg, H. A consistent and accurate ab initio parametrization of density functional dispersion correction (DFT-D) for the 94 elements H-Pu. *J. Chem. Phys.* **2010**, *132*, 154104-154119.

(26) Lu, Q.; Neese, F.; Bistoni, G. Formation of Agostic Structures Driven by London Dispersion. *Angew. Chem., Int. Ed.* **2018**, *57*, 4760-4764.

(27) a) van Lenthe, E.; Ehlers, A.; Baerends, E.-J. Geometry optimizations in the zero order regular approximation for relativistic effects. *J. Chem. Phys.* **1999**, *110*, 8943-8953. b) van Lenthe, E.; Baerends, E. J.; Snijders, J. G. Relativistic total energy using regular approximations. *J. Chem. Phys.* **1994**, *101*, 9783-9792. c) van Lenthe, E.; Baerends, E. J.; Snijders, J. G. Relativistic regular two-component Hamiltonians. *J. Chem. Phys.* **1993**, *99*, 4597-4610.

(28) Perdew, J. P.; Burke, K.; Ernzerhof, M. Generalized Gradient Approximation Made Simple. *Phys. Rev. Lett.* **1996**, *77*, 3865-3868.

(29) a) Hamdaoui, M.; Ney, M.; Sarda, V.; Karmazin, L.; Bailly, C.; Sieffert, N.; Dohm, S.; Hansen, A.; Grimme, S.; Djukic, J.-P. Evidence of a donor–acceptor (Ir–H)→SiR_3 interaction in a trapped Ir(III) silane catalytic intermediate. *Organometallics* **2016**, *35*, 2207-2223. b) Ho Binh, D.; Milovanovic, M.; Puertes-Mico, J.; Hamdaoui, M.; Zaric, S. D.; Djukic, J.-P. Is the R_3Si moiety in metal-silyl complexes a Z ligand ? An answer from the interaction energy. *Chem. Eur. J.* **2017**, *23*, 17058–17069. c) Hamdaoui, M.; Desrousseaux, C.; Habbita, H.; Djukic, J.-P. Iridacycles as catalysts for the autotandem conversion of nitriles into amines by hydrosilylation: experimental investigation and scope. *Organometallics* **2017**, *36*, 4864-4882.

(30) Klamt, A.; Schuurmann, G. COSMO: a new approach to dielectric screening in solvents with explicit expressions for the screening energy and its gradient. *J. Chem. Soc., Perkin Trans. 2* **1993**, 799-805.

(31) a) Contreras-García, J.; Johnson, E. R.; Keinan, S.; Chaudret, R.; Piquemal, J.-P.; Beratan, D. N.; Yang, W. NCIPLOT: A Program for Plotting Noncovalent Interaction Regions. *J. Chem. Theor. Comput.* **2011**, *7*, 625–632. b) Johnson, E. R.; Keinan, S.; Mori-Sánchez, P.;

Contreras-García, J.; Cohen, A. J.; Yang, W. Revealing Noncovalent Interactions. *J. Am. Chem. Soc.* **2010**, 132, 6498–6506.

(32) a) Yang, Y.-F.; Hong, X.; Yu, J.-Q.; Houk, K. N. ExperimentalComputational Synergy for Selective Pd(II)-Catalyzed C–H Activation of Aryl and Alkyl Groups. *Acc. Chem. Res.* **2017**, *50*, 2853-2860. b) Yang, Y.-F.; Chen, G.; Hong, X.; Yu, J.-Q.; Houk, K. N. The Origins of Dramatic Differences in Five-Membered vs Six-Membered Chelation of Pd(II) on Efficiency of C(Sp3)–H Bond Activation. *J. Am. Chem. Soc.* **2017**, *139*, 8514–8521. c) Davies, D. L.; Macgregor, S. A.; McMullin, C. L. Computational Studies of Carboxylate-Assisted C–H Activation and Functionalization at Group 8–10 Transition Metal Centers. *Chem. Rev.* **2017**, *117*, 8649-8709.(

(33) a) Brookhart, M.; Green, M. L. H. Carbon-hydrogen-transition metal bonds. *J. Organomet. Chem.* **1983**, *250*, 395-408. b) Green, M. L. H.; O'Hare, D. The activation of carbon-hydrogen bonds. *Pure Appl. Chem.* **1985**, *57*, 1897-1910. c) Brookhart, M.; Green, M. L. H.; Wong, L. L. In *Carbon-Hydrogen-Transition Metal Bonds*; Lippard, S. J., Ed.; Wiley-Blackwell: 1988; Vol. 36, p 1-124.

(34) a) Trofimenko, S. Boron-Pyrazole Chemistry. IV. Carbon- and Boron-Substituted Poly[(1-pyrazolyl) borates]. *J. Am. Chem. Soc* **1967**, *89*, 6288-6294. b) Trofimenko, S. Molybdenum complexes with non-inert-gas configuration. *J. Am. Chem. Soc* **1968**, *90*, 4754-4755. c) Brookhart, M.; Green, M. L. H.; Parkin, G. Agostic interactions in transition metal compounds. *PNAS* **2007**, *104*, 6908-6914. d) Clot, E.; Eisenstein, O. In *Principles and Applications of Density Functional Theory in Inorganic Chemistry II*; Kaltsoyannis, N., McGrady, J. E., Eds.; Springer Berlin Heidelberg: Berlin, Heidelberg, 2004, p 1-36. e) Lersch, M.; Tilset, M. Mechanistic aspects of C-H activation by Pt complexes. *Chem. Rev.* **2005**, *105*, 2471-2526. f) Crabtree, R. H. Alkane Carbon – Hydrogen Bond Activation. *Transition* **2011**.

(35) a) Ittel, S. D.; Johnson, L. K.; Brookhart, M. Late-metal catalysts for ethylene homo- and copolymerization. *Chem. Rev.* **2000**, *100*, 1169-1203. b) Cherry, S. D. T.; Kaminsky, W.; Heinekey, M. D. Structure of a Novel Rhodium Phosphinite Compound: Agostic Interactions as a Model for an Oxidative Addition Intermediate. *Organometallics* **2016**, *35*, 2165-2169. c) Ritleng, V.; Sirlin, C.; Pfeffer, M. Ru-, Rh-, and Pd-Catalyzed C−C Bond Formation Involving C−H Activation and Addition on Unsaturated Substrates: Reactions and Mechanistic Aspects. *Chem. Commun.* **2002**, *102*, 1731-1770. d) Shteinman, A. A. Coordinational activation of methane and other alkanes by metal complexes. *Russ. Chem. Bull.* **2016**, *65*, 1930-1944. e) Shteinman, A. Activation and selective oxy-functionalization of alkanes with metal complexes: Shilov reaction and some new aspects. *J. Mol. Cat. A* **2017**, *426*, 305-315. f) Toner, A.; Matthes, J.; Gründemann, S.; Limbach, H.-H.; Chaudret, B.; Clot, E.; Sabo-Etienne, S. Agostic interaction and intramolecular proton transfer from the protonation of dihydrogen ortho metalated ruthenium complexes. *PNAS* **2007**, *104*, 6945-6950. g) Reinartz, S.; White, P. S.; Brookhart, M.; Templeton, J. L. Structural characterization of an intermediate in arene C-H bond activation and measurement of the barrier to C-H oxidative addition: A platinum(II) η2-benzene adduct. *J. Am. Chem. Soc* **2001**, *123*, 12724-12725. h) Sajjad, M. A.; Christensen, K. E.; Rees, N. H.; Schwerdtfeger, P.; Harrison, J. A.; Nielson, A. J. New complexity for aromatic ring agostic interactions. *Chem. Commun.* **2017**, *53*, 4187-4190. i) Sajjad, M. A.; Christensen, K. E.; Rees, N. H.; Schwerdtfeger, P.; Harrison, J. A.; Nielson, A. J. Chasing the agostic interaction in ligand assisted cyclometallation reactions of palladium(ii). *Dalton Trans.* **2017**, *46*, 16126-16138.

(36) Bader, R. F. W. *Atoms in Molecules: A Quantum Theory*; Clarendon: Oxford, 1990.

(37) Popelier, P. *Atoms in molecules, an introduction*; Prentice Education: Harlow, England, 2000.

(38) Schnee, G.; Specklin, D.; Djukic, J.-P.; Dagorne, S. Deprotonation of Al_2Me_6 by Sterically Bulky NHCs: Scope, Rationale through DFT Studies, and Application in the Methylenation of Carbonyl Substrates. *Organometallics* **2016**, *35*, 1726-1734.

(39) Bridgeman, A.J.; Cavigliaso, G.; Ireland, L.R.; Rothery, J. The Mayer bond order as a tool in inorganic chemistry. *J. Chem. Soc., Dalton Trans.* **2001**, 2095-2108

(40) Mitoraj, M. P.; Michalak, A.; Ziegler, T. A Combined Charge and Energy Decomposition Scheme for Bond Analysis. *J. Chem. Theor. Comput.* **2009**, *5*, 962–975.

(41) Tsuzuki, S.; Uchimaru, T.; Mikami, M. Intermolecular Interaction between Hexafluorobenzene and Benzene: Ab Initio Calculations Including CCSD(T) Level Electron Correlation Correction. *J. Phys. Chem. A* **2006**, *110*, 2027–2033.

(42) a) Watt, M.; Hardebeck, L. K. E.; Kirkpatrick, C. C.; Lewis, M. Face-to-Face Arene−Arene Binding Energies: Dominated by Dispersion but Predicted by Electrostatic and Dispersion/Polarizability Substituent Constants. *J. Am. Chem. Soc.* **2011**, *133*, 3854–3862. b) Ehrlich, S.; Moellmann, J.; Grimme, S. Dispersion-Corrected Density Functional Theory for Aromatic Interactions in Complex Systems. *Acc. Chem. Res.* **2013**, *46*, 916–926.

(43) Yang, Y.-F.; Hong, X.; Yu, J.-Q.; Houk, K. N. Experimental–Computational Synergy for Selective Pd(II)-Catalyzed C–H Activation of Aryl and Alkyl Groups. *Acc. Chem. Res.* **2017**, *50*, 2853–2860.

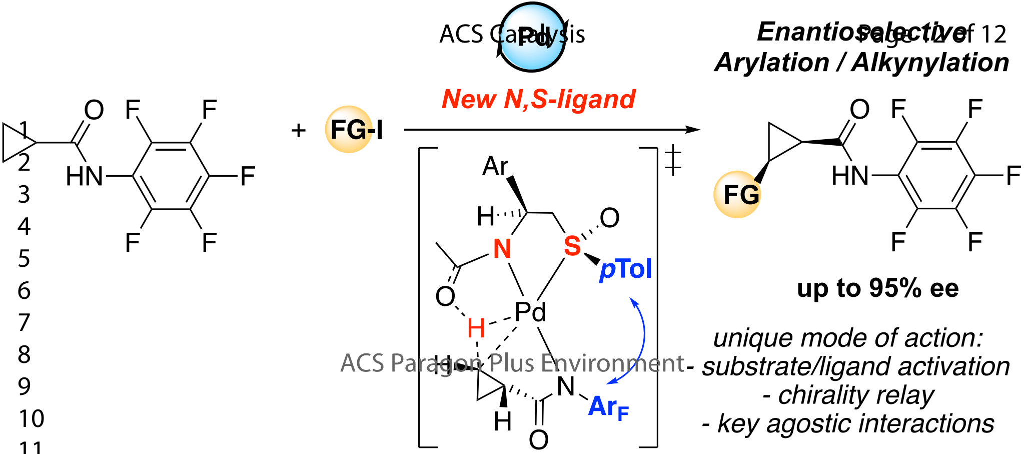
Enantioselective
Arylation / Alkynylation
New N,S-ligand
Pd
FG-I
FG
Ar
H
O
S
N
pTol
Pd
H
N
Ar_F
‡
up to 95% ee
unique mode of action:
- substrate/ligand activation
- chirality relay
- key agostic interactions